Research article

LUMINESCENCE
The Journal of Biological and Chemical Luminescence

Received: 12 May 2014, Revised: 24 July 2014, Accepted: 25 August 2014 Published online in Wiley Online Library

(wileyonlinelibrary.com) DOI 10.1002/bio.2773

Investigations on the interactions of DiAmsar with serum albumins: Insights from spectroscopic and molecular docking techniques

Zari Hooshyar,* Ghasem Rezanejade Bardajee,* Nahaleh Kakavand, Mohaddeseh Khanjari and Nastaran Dianatnejad

ABSTRACT: Diamine-sarcophagine (DiAmsar) binding to human serum albumin (HSA) and bovine serum albumin (BSA) was investigated under simulative physiological conditions. Fluorescence spectra in combination with Fourier transform infrared (FT-IR), UV-visible (UV–vis) spectroscopy, cyclic voltammetry (CV), and molecular docking method were used in the present work. Experimental results revealed that DiAmsar had an ability to quench the HSA and BSA intrinsic fluorescence through a static quenching mechanism. The Stern–Volmer quenching rate constant (K_{sv}) was calculated as $0.372 \times 10^3\ M^{-1}$ and $0.640 \times 10^3\ M^{-1}$ for HSA and BSA, respectively. Moreover, binding constants (K_a), number of binding sites (n) at different temperatures, binding distance (r), and thermodynamic parameters (ΔH°, ΔS°, and ΔG°) between DiAmsar and HSA (or BSA) were calculated. DiAmsar exhibited good binding propensity to HSA and BSA with relatively high binding constant values. The positive ΔH° and ΔS° values indicated that the hydrophobic interaction is main force in the binding of the DiAmsar to HSA (or BSA). Furthermore, molecular docking results revealed the possible binding site and the microenvironment around the bond. Copyright © 2014 John Wiley & Sons, Ltd.

Keywords: DiAmsar; serum albumin; molecular docking; fluorescence quenching

Introduction

Diamine-sarcophagine (DiAmsar; Fig. 1) has been studied extensively, since the first synthesis of unsubstituted sarcophagine in the 1970s (1–4). DiAmsar is able to form conformationally rigid and shaped complexes with a variety of inorganic and organic cations, and by reaction with some anionic and neutral organic and biological substrates gives supramolecular compounds with specific properties and applications (5–8). The obtainable evidence also indicated that the DiAmsar is not toxic (3,5). It is not able to bind alkali or alkaline earth elements in water and therefore does not influence sodium or potassium metabolism, nor do they influence calcium metabolism (7,8). From a biopharmaceutical point of view, one of the most important applications of DiAmsar is in detoxifying biological systems. For example, it is widely used to treat Wilson's disease, in which children have a congenital inability to eliminate copper ions (9,10). Moreover, DiAmsar with basic nitrogen donors showed enhanced thermodynamic and kinetic stability as compared with their noncyclic chelate ligands, and have applications in modern chemical techniques such as magnetic resonance imaging, imaging with radioisotopes and radiotherapy (10–13). Due to the countless possible pharmacological applications of DiAmsar, there have been growing interests in the interactions between DiAmsar and biomolecules (14–16). However, to date there is no report about the interaction between DiAmsar and serum albumins so far.

Serum albumins are the major soluble protein constituents of the circulatory system and have many physiological functions. The most outstanding function of serum albumins is that they serve as depot proteins and transport proteins for many exogenous compounds (17,18). Serum albumins comprise three homologous helical domains (I–III), which are divided into A and B subdomains (19–24). These subdomains can accommodate various compounds, such as a large number of ligands (18). Serum albumins, especially bovine (BSA) and human (HSA), have been extensively studied due to their significance in the pharmacology field (21). Both HSA and BSA display approximately 80% sequence homology and a repeating pattern of disulfides. HSA only has one tryptophan (Trp 214) in subdomain IIA, whereas BSA has two tryptophan moieties (Trp 135 and Trp 214), located in subdomains IA and IIA, respectively (19,22). Many reports have shown that the intrinsic fluorescence of HSA and BSA appears at 350 and 345 nm, re-

* Correspondence to: Zari Hooshyar or Ghasem Rezanejade Bardajee. Department of Chemistry, Payame Noor University (PNU), P.O. BOX, 19395–3697, Tehran, Iran. Tel.: +98 281 3336366; Fax: +98 281 3344081; E-mail: rezanejad@pnu.ac.ir; zhooshyar@gmail.com

Department of Chemistry, Payame Noor University (PNU), P.O. BOX19395-3697, Tehran, Iran

Abbreviations: BSA, bovine serum albumin; CV, cyclic voltammetry; FRET, fluorescence resonance energy transfer; HSA, human serum albumin; LGA, Lamarckian genetic algorithm; NMR, nuclear magnetic resonance; PDB, Protein Data Bank; PET, positron emission tomography; UV, UV-visible; VMD, visual molecular dynamics.

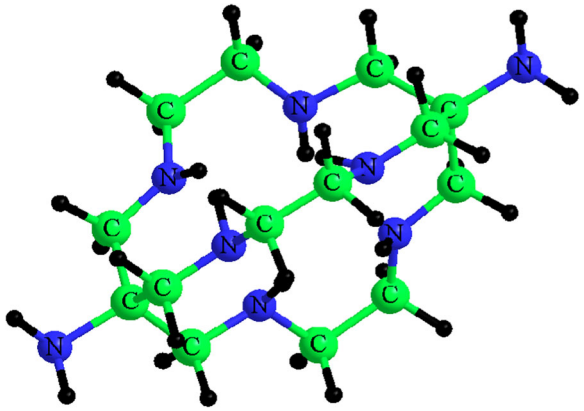

Figure 1. Molecular structure of DiAmsar.

spectively, when excited at 295 nm. These phenomena originate from the aromatic L-amino acid Trp residues (23). The intrinsic fluorescence characteristics are very sensitive to the microenvironment of the fluorescent residues or changes in the local surroundings of serum albumins, such as conformational transition, biomolecular binding and denaturation (17). Therefore, information on interactions of serum albumins and other substances can be obtained by measuring fluorescence of serum albumins (18). However, to elucidate more information and confirm the fluorescence results, other spectroscopies have been applied (24).

In this work, we present the results of a study on the biophysical interactions of DiAmsar with serum albumins (i.e., HSA and BSA) by using several experimental techniques via fluorescence, Fourier transform infrared (FT-IR) and UV-visible (UV–vis) spectroscopy, and cyclic voltammetry (CV). In addition, the aforementioned interactions were modeled by molecular docking methods. This information can provide a fundamental concept for understanding the basic forces involved in the interactions of DiAmsar with HSA and BSA.

Experimental

Reagents

Ethanol, tri(ethylenediamine) cobalt(III)chloride dihydrate, formaldehyde, sodium hydroxide, hydrochloric acid, methanol, stannous chloride dihydrate, hydrochloric acid, sodium hydroxide, cobalt (II) chloride, sodium cyanide, fatty acid and globulin-free bovine serum albumin (BSA) and human serum albumin (HSA) were obtained from Sigma-Aldrich Chemicals and used without further purification. Tris(hydromethyl)aminomethane (Tris) was purchased from Acros (Geel, Belgium). Double distilled water was used in all experiments.

Apparatus

The UV–vis spectra were recorded at room temperature on a Shimadzu UV-visible 1650 PC spectrophotometer equipped with 1.0 cm quartz cells. Fluorescence measurements were carried out in a SCINCO's fluorescence spectrometer FluoroMate FS-2, using quartz cuvette with 1 cm optical path-length and both band widths were set at 5 nm. ^{1}H nuclear magnetic resonance (NMR) and ^{13}C NMR spectra were recorded at 400 MHz with a Varian Mercury 400 spectrometer and a Bruker Avance III spectrometer, respectively, using deuterium oxide as solvent. The FT-IR spectra were carried out on a Jasco 4200 FT-IR spectrophotometer. Voltammetric measurements were made with a computer controlled electrochemical system by AUTULAB PGSTAT12. A glassy carbon electrode was used as a working electrode and a platinum wire served as the auxiliary electrode. The reference electrode was an AgCl/Ag.

Preparation of DiAmsar

DiAmsar was synthesized by the Sargeson procedure (4,13) as described follows (Scheme 1):

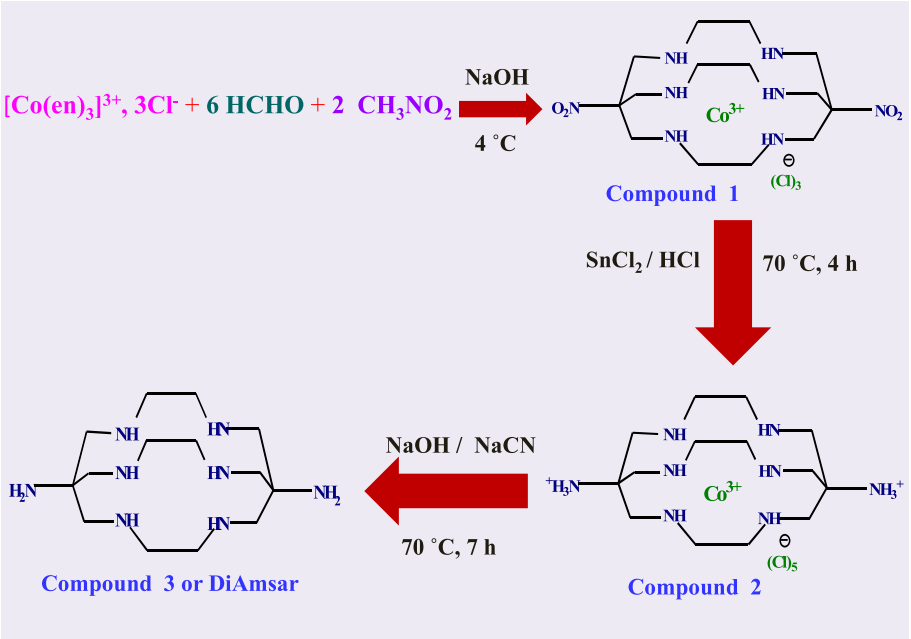

Scheme 1. General route for the synthesis of DiAmsar.

LUMINESCENCE
The Journal of Biological and Chemical Luminescence

- Compound 1: The complex of tri(ethylenediamine) cobalt(III) chloride dihydrate (1 eq, 2 g) was dissolved in a mixture of water (3 mL) and aqueous formaldehyde 37 % (10.4 eq, 4.5 mL). Then, nitromethane (3.45 eq, 1.06 mL) was added to the solution. The resulting solution was cooled at 4 °C in an ice-water bath. Aqueous sodium hydroxide (4 M, 3.45 eq, 5 mL) was cooled to 4 °C and mixed with the resulting solution above. The combined solution was stirred magnetically for 90 min in an ice-water bath while maintaining the temperature at 4 °C. The mixture rapidly turned deep brown from the initially orange colour. After 90 min, the reaction temperature was allowed to come to room temperature. At the end, the reaction was quenched by the addition of concentrated hydrochloric acid (HCl 37%, 60 mmol, 5 mL). The orange precipitate was collected by filtration after cooling on ice for 90 min, and washed with methanol. Then, the orange powder was dried at room temperature. (^{1}H NMR (400 MHz, D_2O) δ (ppm): 2.94–2.96 (d, J = 8 Hz, 6H, -NH-CH_2-CH_2-NH-), 3.36–3.40 (d, J = 11 Hz, 6H, -NH-CH_2-C-NO_2), 3.58–3.60 (d, J = 8 Hz, 6H, -NH-CH_2-CH_2-NH-), 3.89–3.93 (d, J = 11 Hz, 6H, -NH-CH_2-C-NO_2). ^{13}C NMR (400 MHz, D_2O) δ (ppm): 51.28, 54.62, 87.53. HRMS (EI, m/z) calcd. for $C_{14}H_{31}CoN_8O_4$ 431.3565 $[M - 3\ HCl]^+$, found 431.2689).
- Compound 2: The stannous chloride dihydrate (13 eq, 3 g) was introduced into a round bottom flask under nitrogen atmosphere. Then, concentrated hydrochloric acid (37%, 145 eq, 12 mL) was added followed by the addition of ethanol (6 mL). The resulting solution was stirred magnetically and heated to 70 °C under nitrogen until the solution became colourless. Then, the compound 1 complex (1 eq, 600 mg) was added to the solution under strong stirring. The resulting solution was heated at 70 °C for 4 h. The colour of the solution turned green from orange/brown and then, became darker. After that, water (6 mL) was added to the solution, and it turned orange. The solution was cooled at room temperature for 15 min before the flask was immersed in an ice-water bath. The orange precipitate formed was filtered and dried. The $[Co\text{-}(NH_3)_2\text{-}sar]^{5+}$,$Cl_5$ complex was obtained with a yield around 90%. (^{1}H NMR (400 MHz, D_2O) δ (ppm): 2.93–2.97 (m, 12H, -NH-CH_2-CH_2-NH-), 3.51–3.57 (m, 12H, -NH-CH_2-C-NH_3^+). ^{13}C NMR (400 MHz, D_2O) δ (ppm): 51.4, 54.7, 58.5).
- Compound 3 or DiAmsar: sodium hydroxide (2.11 eq, 77 mg) was dissolved in deoxygenated water (7 mL) and the solution was placed under nitrogen to eliminate oxygen. The bubbling was continued for 30 min. Then, compound 2 complex (1 eq, 500 mg) and cobalt (II) chloride (1.01 eq, 118 mg) were dissolved in the basic solution. After homogenization of the solution, sodium cyanide (17.7 eq, 783 mg) was added to the resulting solution under strong stirring. The mixture was heated to 70 °C and vigorously stirred under nitrogen until the solution had become almost yellow (~7 h). The final solution was dried under air flow, and the residue was extracted with boiling acetonitrile (three-fold, 10 mL). The total extract was reduced under vacuum (10 mL), and cooled to −10 °C to precipitate white crystals of the product. The product was recovered by filtration and dried for further experiments. (^{1}H NMR (400 MHz, D_2O) δ (ppm): 2.80 (s, 12 H, -NH-CH_2-CH_2-NH-), 2.88 (s, 12 H, -NH-CH_2-C-NH_2). ^{13}C NMR (400 MHz, D_2O) δ (ppm): 48.1, 51.7, 57.4. HRMS (EI, m/z) calcd. for $C_{14}H_{34}N_8$ 315.4813 $[M + H]^+$, found 315.3858).

Procedure

Tris–HCl buffer solution (pH = 7.40) consisted of 0.1 M Tris and was adjusted to pH = 7.40 by 36% HCl. NaCl (0.10 M) was dissolved in Tris–HCl buffer solution (pH = 7.40) to keep the ionic strength. Appropriate amounts of HSA and BSA were directly dissolved in pH 7.40 Tris–HCl buffers to prepare HSA and BSA stock solutions with 1.0×10^{-5} M concentrations of HSA and BSA. These stock solutions were kept at below 4 °C.

For absorption titration experiments, appropriate quantities of HSA and BSA solutions (5.0×10^{-6} M) were transferred to a 1-cm path-length cuvette, and then different amounts of DiAmsar solution were added and diluted to 2 mL with Tris–HCl buffer. Absorbance spectra were recorded in the range of 200–800 nm after each successive addition of DiAmsar and equilibration (ca. 5 min) with blanks of Tris–HCl buffer.

For fluorescence titration experiments, HSA and BSA solutions (2 mL, 5.0×10^{-6} M) were placed in a quartz cuvette and titrated with various amounts of DiAmsar. The fluorescence emission spectra were recorded in the range of 310–540 nm at the excitation wavelength (λ_{ex}) of 295 nm.

For voltammetric measurements, first a blank CV was run with the Tris–HCl buffers, HSA, and BSA at 298 K, which showed no electroactivity in the potential range of our interest (−1.15 V to 0.25 V). Cyclic voltammograms of DiAmsar were recorded from −1.15 V to 0.25 V before and after the addition of different volumes of the stock HSA and BSA solutions corresponding to the final concentration of HSA, and BSA ranging from 1.8×10^{-5} M to 4.2×10^{-5} M within the cell. Prior to the measurement, the GC electrode was polished with 0.1 mm alumina powder and washed with distilled water. The voltage scan rate was set at 100 mV/s.

Molecular docking

The crystal structures of HSA (PDB Code: 2BXN) and BSA (PDB Code: 4F5S) were downloaded from the Protein Data Bank (PDB). The 3D structure of the DiAmsar was made using Gauss view 5.0. The geometry of DiAmsar was optimized using Gaussian 03. The binding interactions of DiAmsar with HSA and BSA were simulated by molecular docking using AutoDock 4.0 (25). The partial atomic charges of DiAmsar and proteins were calculated using Kollman (26) and Gasterier methods (25), respectively. The Lamarckian genetic algorithm (LGA) was selected for the conformational search, and all parameters were the same for each docking. The grid maps ($90 \times 90 \times 90$ Å) were then calculated using Auto Grid with a grid-point spacing of 0.375 Å for DiAmsar, which ensured an appropriate size of DiAmsar accessible space (26). The number of genetic algorithm run and the number of evaluations were set to 200 and 2.5 million, respectively. Other docking parameters were set as default. The dominating configuration of the binding complex of DiAmsar with HSA and BSA with minimum binding energy was selected. Finally, visualization of the docked pose was carried out using PyMol and visual molecular dynamics (VMD) molecular graphic programs.

Results and discussions

Proton NMR spectra of compound 1, 2, and 3 are shown in Fig. 2. As can be seen in the ^{1}H NMR of compound 1, there are four massive doublets including two doublets of doublets, which are characteristic of protons near the quaternary carbons. And, the two

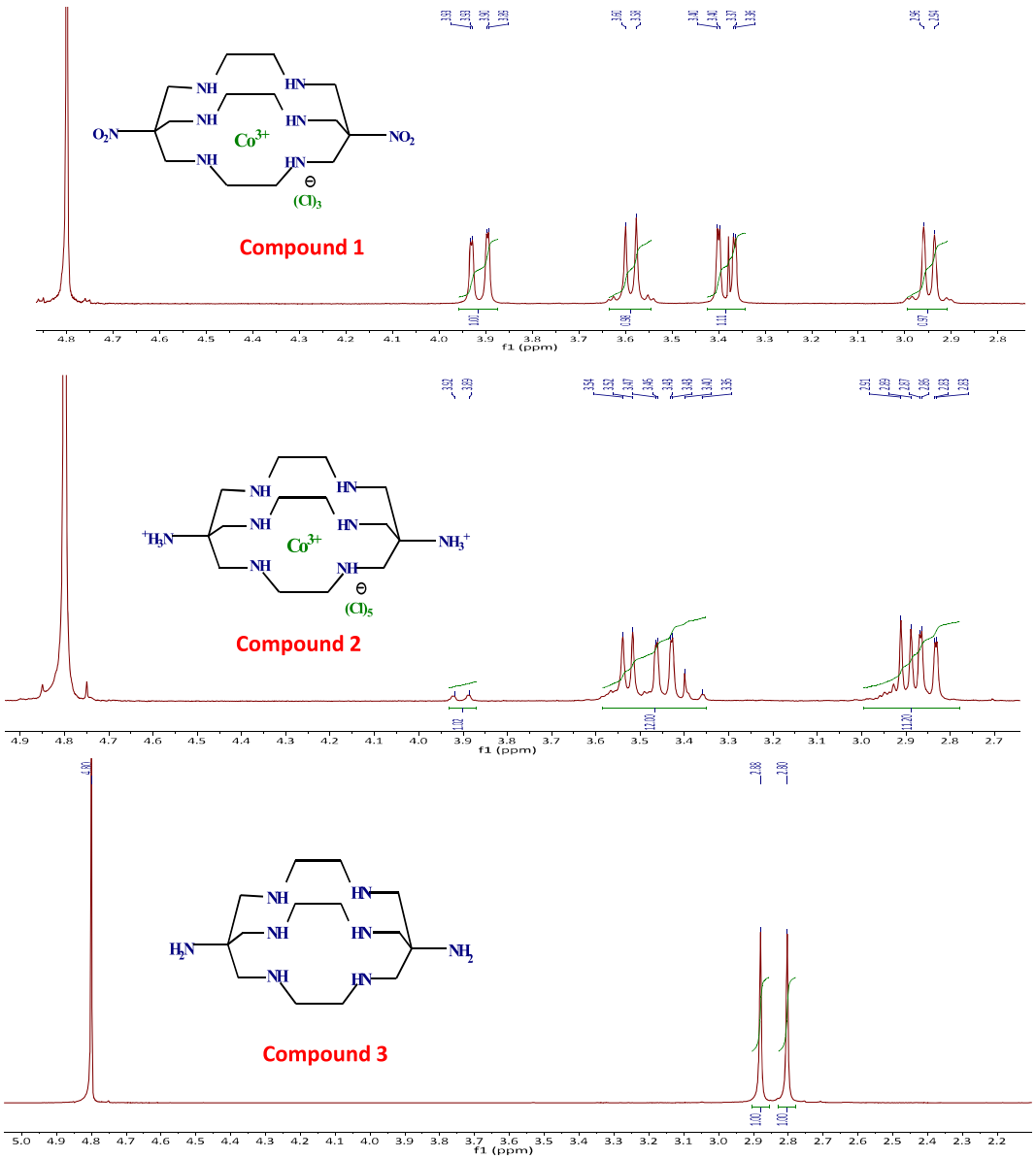

Figure 2. ^{1}H NMR spectra of compound 1, 2, and 3.

remaining doublets are characteristic of protons between the secondary amines. ^{1}H NMR spectra of the compound 2 shows two multiplets at 2.83–2.91 ppm and 3.40–3.54 ppm corresponding to the -CH_2 between the secondary amines and the -CH_2 close to the ammonium groups, respectively. Each multiplet integrates for 12 protons due to the symmetry of the molecule. At 3.89–3.92 ppm, a doublet was observed that characterizes the presence of compound 2. Thus, 8% of unreacted complex remains in the recovered product. ^{1}H NMR spectra of the compound 3 or DiAmsar showed two singlet at 2.76 ppm and 2.85 ppm corresponding to the -CH_2 between the secondary amines and the -CH_2 close to the primary amines, respectively. Each singlet integrates for 12 protons due to the symmetry of the molecule.

Moreover, compounds 1, 2, and 3 were characterized by mass spectrometry and results are shown in Fig. 3. It is clear from the mass spectrum of compound 1 that there is a single peak of m/z equal to 431.2. The position of this peak corresponds to the molar mass of compound 1 from which three molecules of HCl has been removed (to get a neutral compound without counter ion). The removal of the molecules of HCl is induced by sample preparation for the analysis (insertion in the matrix for ionization). The obtained m/z corresponds to the molar mass of the neutral compound plus one proton due to ionization. A mass spectrum of compound 2 contains a main peak of m/z equal to 371.2. During the process of sample preparation, compound 2 lost five molecules of HCl to result in a neutral compound without counter ion. The main peak corresponded to the molar mass of the neutral compound plus one proton due to ionization. A low peak of m/z equal to 407.2 was observed and characterized the molar mass of compound 2, which lost four HCl and got one proton. The mass spectrum of compound 3 showed a single peak of m/z equal to 315.3. This peak corresponded to the molar mass of compound 3 or DiAmsar plus one proton due to ionization

UV–vis spectroscopy studies

UV–vis spectroscopy is a very simple and applicable method to explore the structural change and to characterize the complex

LUMINESCENCE
The Journal of Biological and Chemical Luminescence

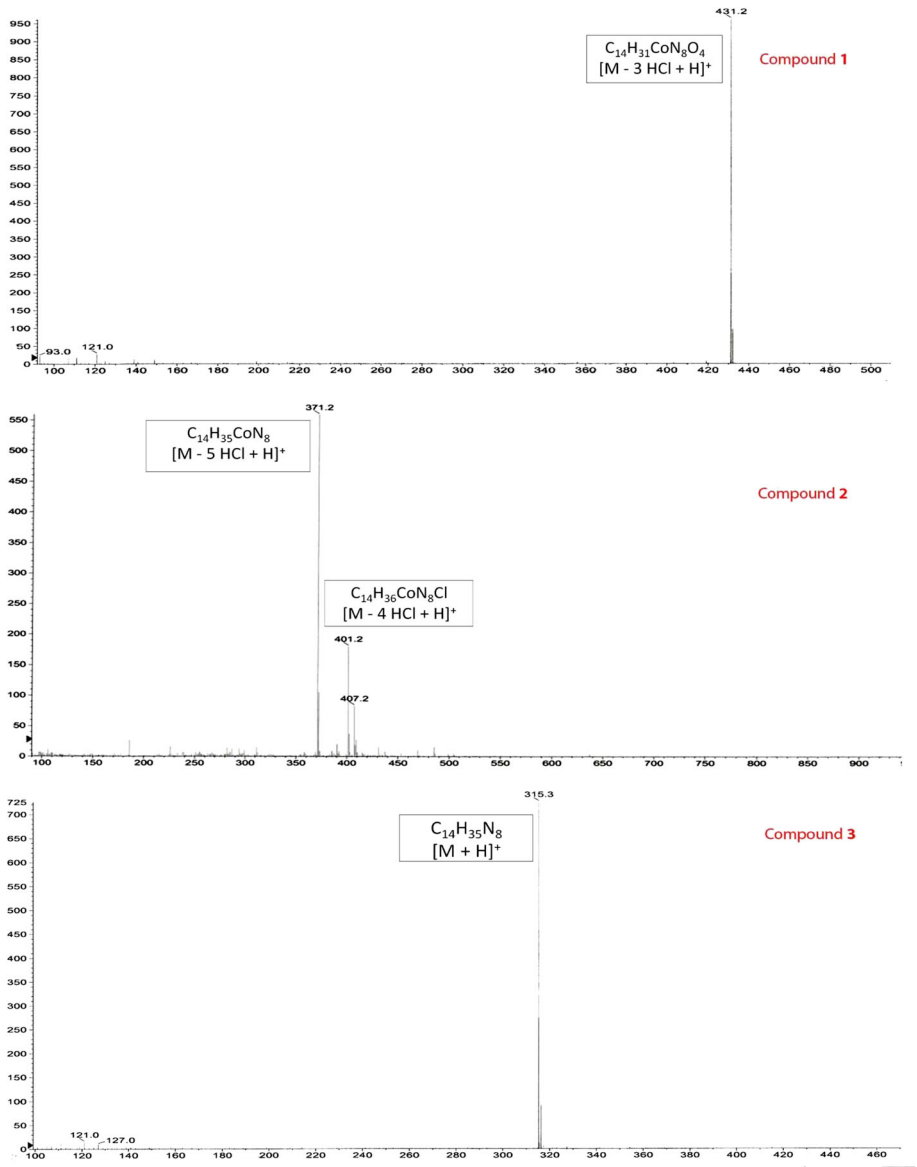

Figure 3. Mass spectra of compound 1, 2, and 3.

formation (20,23). Figure 4 shows the effect of DiAmsar on the UV–vis spectra of HSA and BSA. As shown in Fig. 4, strong absorption peaks were observed at 280 nm and the peaks intensity increased with the addition of DiAmsar. From this study we observed that upon increasing the concentration of DiAmsar, the absorbance of HSA and BSA increased regularly without change in its absorption wavelength (280 nm).

The obvious enhancement of absorbance intensity indicated the formation of a new complex between DiAmsar and HSA (or BSA). The equilibrium for the formation of complex between DiAmsar and HSA (or BSA) is given by equation 1, where K_a represents the apparent association constant:

$$\text{HSA (or BSA)} + \text{DiAmsar} \leftrightarrow \text{HSA (or BSA)}.....\text{DiAmsar}$$
$$K_a = [\text{HSA (or BSA)}.....\text{DiAmsar}]/([\text{HSA (or BSA)}][\text{DiAmsar}]) \quad (1)$$

The changes in intensity of the absorption peak (280 nm) as a result of formation of the surface complex were utilized to obtain K_a according to the method reported by Benesi and Hildebrand (22):

$$A_{obs} = (1-\alpha)C_0\varepsilon_{HSA}1 + \alpha C_0\varepsilon_C 1 \quad (2)$$

where A_{obs} is the observed absorbance of the solution containing different concentrations of DiAmsar at 280 nm, α is the degree of association between DiAmsar and HSA (or BSA), ε_{HSA} and ε_c are the molar extinction coefficients at the defined wavelength ($\lambda = 280$ nm) of HSA (or BSA) and the formed complex, respectively. Equation 2 can be expressed as equation 3, where A_0 and A_c are the absorbance of HSA (or BSA) and the complex at 280 nm, respectively, with the concentration of C_0:

$$A_{obs} = (1-\alpha)A_0 + \alpha A_C \quad (3)$$

At relatively high DiAmsar concentrations, α can be equated to (K_a [DiAmsar])/(1 + Ka[DiAmsar]). In this case, equation 3 can be changed to the following equation:

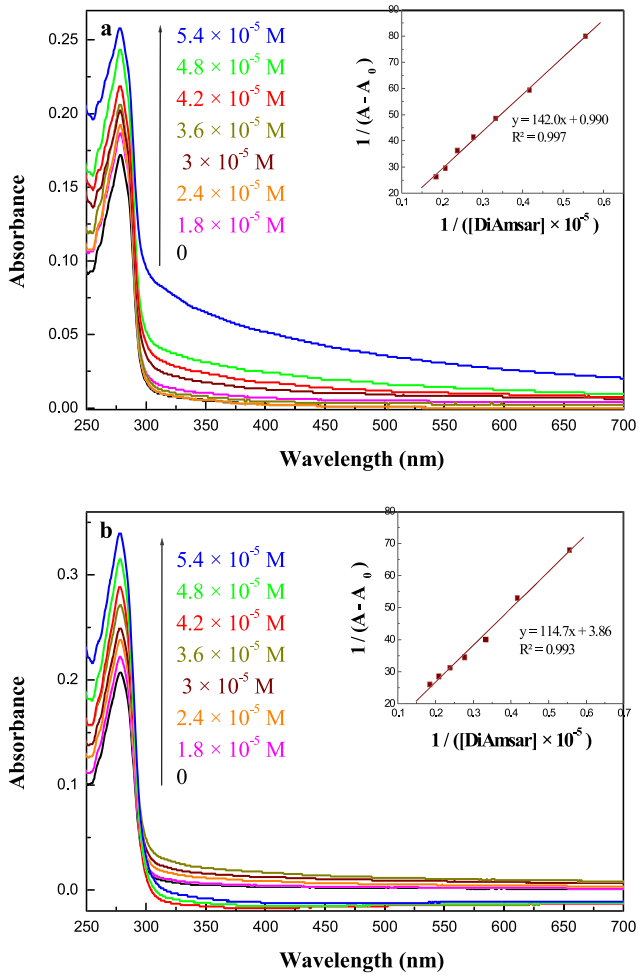

Figure 4. Absorption spectra of (a) HSA and (b) BSA in the absence and presence of DiAmsar in the concentration range of 0–5.4 × 10^{-5} M. Insert shows the straight line dependence of 1/(A – A_0) on the reciprocal concentration of DiAmsar.

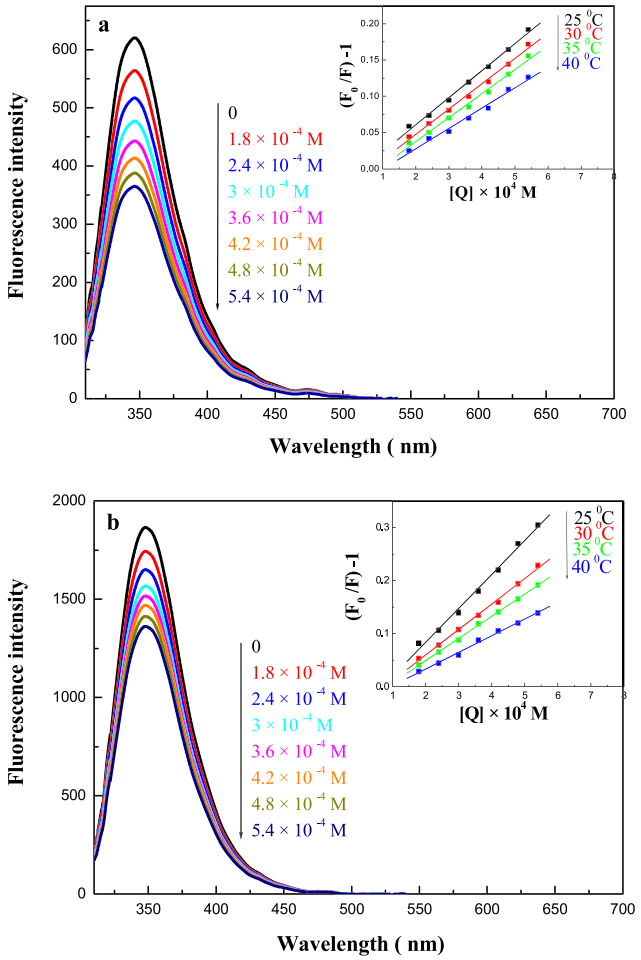

Figure 5. Fluorescence quenching spectra of (a) HSA and (b) BSA with DiAmsar. Insert: Stern–Volmer curves for the binding of HSA and BSA with DiAmsar at different temperatures (λ_{ex} = 295).

$$1/(A_{obs} - A_0) = 1/(A_c - A_0) + 1/(K_a(A_c - A_0)[DiAmsar]) \quad (4)$$

The enhancement of absorbance at 280 nm was due to absorption of surface complex, based on the linear relationship between $1/(A_{obs} - A_0)$ vs. reciprocal concentration of colloidal DiAmsar with a slope equal to $1/K_a$ $(A_c - A_0)$ and an intercept equal to $1/(A_c - A_0)$ (Fig. 4, insert). The value of apparent association constant (K_a) determined from this plot is 0.698×10^3 and 3.365×10^3 M^{-1} for HSA and BSA, respectively.

Fluorescence spectroscopy studies

Fluorescence spectroscopy was used to monitor changes on the tertiary structure of HSA and BSA, induced by the interaction with DiAmsar. These interactions can, in principle, produce changes in the position or orientation of the tryptophan residues, altering their exposure to solvent, and leading to alterations on the quantum yield (21). Figure 5 shows the obvious intrinsic fluorescence of HSA and BSA molecules around 350 and 345 nm, respectively. As can be seen in this figure, a quenching of fluorescence occurs with the addition of DiAmsar. Also, under the same condition, no fluorescence of DiAmsar was observed. These results indicated that the binding of DiAmsar to HSA and BSA, quenched the intrinsic fluorescence of the tryptophan residue in HSA and BSA. The fluorescence quenching effect was due to the formation of a non-fluorescent complex (18,27).

Fluorescence quenching could proceed via different mechanisms, usually classified as dynamic quenching and static quenching (20,23). Dynamic and static quenching can be distinguished by their different dependence on temperature. Higher temperatures will result in faster diffusion and hence larger amounts of collisional quenching and higher temperatures will typically result in the dissociation of weakly bound complexes and hence smaller amounts of static quenching. The linear Stern–Volmer equation is commonly used to identify whether or not the quenching is caused by dynamic collision or formation of complex. The linear Stern–Volmer equation can be described as follows (28,29):

$$F/F_0 = 1 + K_q\tau_0[Q] = 1 + K_{SV}[Q] \quad (5)$$

where F_0 and F represent the fluorescence intensities in the absence and in the presence of quencher, K_q is the quenching rate constant of the bimolecular, K_{SV} is the dynamic quenching constant, τ_0 is the average lifetime of the molecule without quencher, and [Q] is the concentration of the quencher. The Stern–Volmer curves of F_0/F versus [Q] at different temperatures

LUMINESCENCE
The Journal of Biological and Chemical Luminescence

are shown in Fig. 5 and the calculated K_{SV} and k_q values are presented in Table 1. The plots showed that within the investigated concentration, the results exhibited a good linear relationship. Table 1 shows that K_{SV} values were inversely correlated with temperatures, which suggested that the fluorescence quenching of HSA and BSA were initiated by the formation of ground-state complex (20). Furthermore, k_q values were much greater than the maximum scatter collision quenching constant ($2.0 \times 10^{10}\ M^{-1}\ S^{-1}$) for various quenchers with biomolecules, (20,23). Considering that in our experiment the rate constants of the protein quenching procedure initiated by DiAmsar were higher than the maximum value possible for diffusion limited quenching in solution (~$10^{10}\ M^{-1}\ S^{-1}$). It suggested that the static quenching was dominant in the interaction between DiAmsar and HSA (or BSA).

From the above results, it is seen that the fluorescence quenching from DiAmsar-HSA (or BSA) complexes is a static quenching process, hence the equilibrium between free and bound molecule can be expressed by the following double-logarithm regression equation (24,28):

$$\mathrm{Log}((F_0 - F)/F) = \log K_a + n \log\ [Q] \qquad (6)$$

where K_a and n are the binding constant and the number of binding sites, respectively. From equation 6, the binding parameters can be obtained by a plot of log [(F_0 – F)/F] versus log[Q] (Fig. 6). The values of K_a and n at 298, 303, 308 and 313 K are listed in Table 1. These results indicated complex formation between DiAmsar and HSA (or BSA) on the order of $10^3\ M^{-1}$, six orders of magnitude smaller than previously studied BSA-fluorescein sodium salt complexes and an order of magnitude smaller than HSA–indomethacin system (30,31).

These differences in the overall value may result from structure effects of fluorescein sodium salt, indomethacin, and DiAmsar. The binding site ($n = 1$) increased slightly with the rising temperature, which showed the interaction of DiAmsar with HSA (or BSA), indicating the presence of one high affinity binding site. Moreover, the interaction between DiAmsar and HSA (or BSA) accelerated with the temperature. Hence the high affinity binding site of the interaction is slightly strengthened (24,28). The results indicated that there is one class of binding site for HSA and BSA. The fact that the binding constant between DiAmsar and HSA (or BSA) increased with increasing temperature suggested that there was a strong interaction between DiAmsar and HSA (or BSA). This clearly implied that DiAmsar would be bound, stored and transported by HSA and BSA in the body (20).

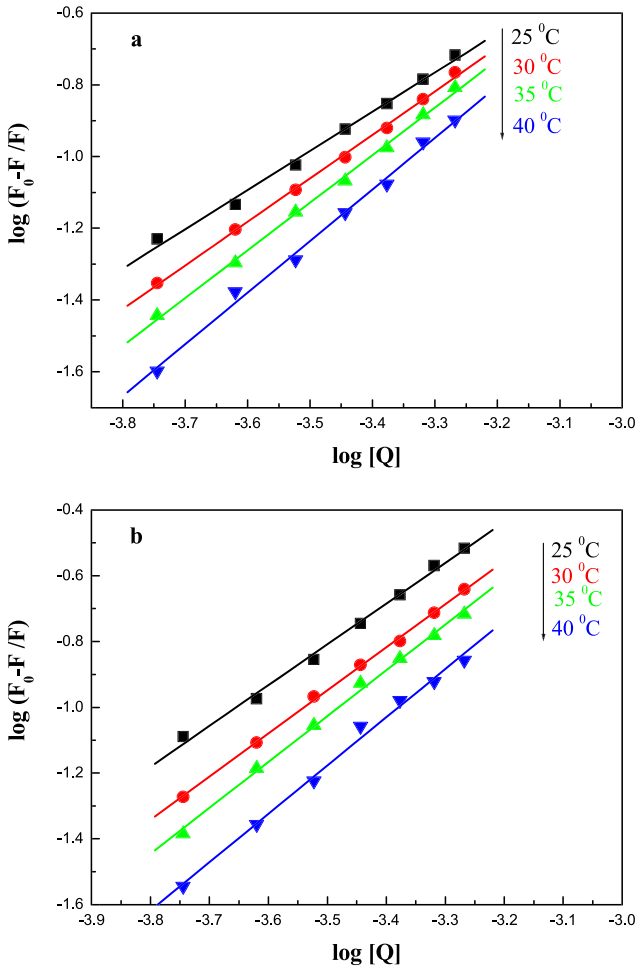

Figure 6. The plots of log ((F_0 – F)/F) versus log [Q] for (a) HSA and (b) BSA at three different temperatures.

The interaction forces between a ligand and a biomolecule may involve hydrophobic forces, electrostatic interactions, van der Waals interactions, hydrogen bonds, etc. (22,29). According to the data of enthalpy change (ΔH°) and entropy change (ΔS), the model of interaction between a ligand and a biomolecule can be concluded (24): $\Delta H° > 0$ and $\Delta S° > 0$, hydrophobic forces, (2) $\Delta H° < 0$ and $\Delta S° < 0$, van der Waals interactions and hydrogen bonds, and (3) $\Delta H° < 0$ and $\Delta S° > 0$, electrostatic interactions. In order to elucidate the interaction of DiAmsar with HSA and BSA, we calculated the thermodynamic parameters from

Table 1. The Stern–Volmer constants (K_{SV}), quenching constants (K_q), binding constants (K_a), number of binding sites (n), and relative thermodynamic parameters in the interaction between DiAmsar and HSA (or BSA) at different temperatures

Serum albumin	T (K)	K_{SV} ($10^3\ M^{-1}$)	K_q ($10^{11}\ M^{-1}\ S^{-1}$)	R^a	K_a ($10^3\ M^{-1}$) double-logarithm equation	n^b	R^a
HSA	298	0.372	0.372	0.994	0. 695	1.093	0.994
	303	0.348	0.348	0.993	1.542	1.214	0.998
	308	0.330	0.330	0.990	3.311	1.328	0.997
BSA	313	0.280	0.280	0.987	6.324	1.439	0.994
	298	0.640	0.640	0.992	3.380	1.239	0.994
	303	0.480	0.480	0.996	4.315	1.309	0.999
	308	0.418	0.418	0.999	7.095	1.393	0.996
	313	0.314	0.314	0.994	9.205	1.438	0.993

equations (7–9). If the temperature does not vary significantly, the enthalpy change (ΔH°) can be regarded as a constant. The free energy change (ΔG°) can be estimated from the following equation (23):

$$\ln K_a = -\Delta H^\circ/RT + \Delta S^\circ/R \quad (7)$$

$$\Delta G = \Delta H^\circ - T\Delta S^\circ \quad (8)$$

where R is the gas constant, T is the experimental temperature, and K_a is the binding constant at the corresponding T. The relative thermodynamic parameters for the interaction of DiAmsar with HSA and BSA are shown in Table 2. The negative sign for ΔG° means that the interaction process is spontaneous. The positive ΔH° and positive ΔS° values indicated that hydrophobic forces might play a major role in the binding between DiAmsar and HSA (or BSA).

Quite a lot of information concerning molecular details of donor–acceptor pair can be had from non-radiation energy transfer (19). Fluorescence resonance energy transfer (FRET) occurs when the emission spectrum of the donor overlaps the absorption spectrum of the acceptor. The dependence of energy transfer rate on interaction distance has been widely used to measure the distance between the donor and the acceptor. Generally, the maximum distance is in the range of 1–10 nm. According to Fröster non-radiation energy (19,20), energy transfer is related not only to the distance between the acceptor and donor, but also to the critical energy transfer distance (R_0) as follows:

$$E = R_0^6/(R_0^6 + r^6) \quad (9)$$

where R_0 is the critical transfer distance when the transfer efficiency is 50%, and r is the mean distance between the centers of the donor and acceptor diploes. Here the donor and

Table 2. Thermodynamic parameters of the DiAmsar-HSA (or BSA) systems at different temperatures

Serum albumin	T (K)	ΔS° (J mol^{-1} K^{-1})	ΔH° (kJ mol^{-1})	ΔG° (kJ mol^{-1})
HSA	298	439.312	11.466	-11.945
	303	439.312	11.466	-12.164
	308	439.312	11.466	-12.384
BSA	313	439.312	11.466	-12.604
	298	249.421	54.298	-74.273
	303	249.421	54.298	-75.520
	308	249.421	54.298	-76.767
	313	249.421	54.298	-78.014

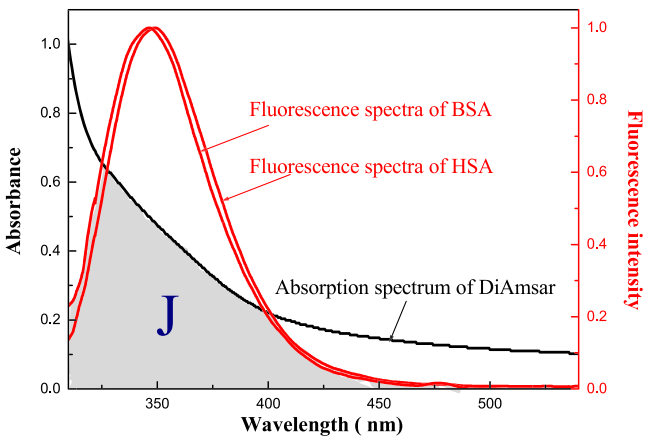

Figure 7. Spectral overlap of DiAmsar absorption with HSA and BSA fluorescence.

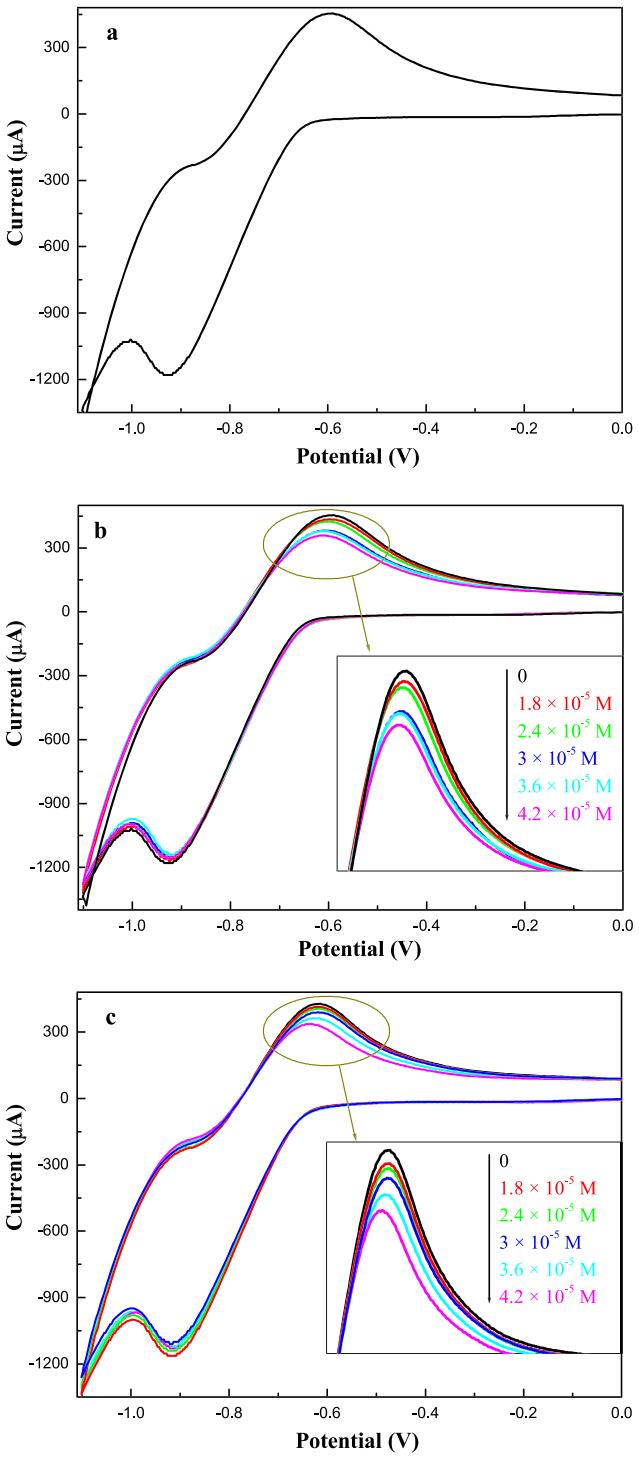

Figure 8. CV curves of DiAmsar in (a) absence, and presence of different concentrations of (b) HSA and (c) and BSA at T = 298 K.

LUMINESCENCE
The Journal of Biological and Chemical Luminescence

acceptor are HSA (or BSA) and DiAmsar, respectively. E is the energy transfer efficiency calculated using equation 10:

$$E = 1 - (F/F_0) \quad (10)$$

where F and F_0 are the fluorescence intensity of HSA (or BSA) in the presence and absence of DiAmsar, respectively. And R_0 can be given by:

$$R_0^6 = 8.8 \times 10^{-25} \kappa^2 n^{-4} \Phi J \quad (11)$$

where κ^2 is the special orientation factor of the dipole; n is the refractive index of the medium, Φ is the fluorescence quantum yield of the donor in the absence of the acceptor. J expresses the overlap integral of the fluorescence emission spectrum of the donor and the absorption spectrum of the acceptor. J is given by:

$$J(\lambda) = \sum F(\lambda)\varepsilon_A(\lambda)\left(\lambda^4 \Delta\lambda / \sum F(\lambda)\,\Delta\lambda\right) \quad (12)$$

where $F(\lambda)$ is the fluorescence intensity of donor at wavelength λ, and $\varepsilon_A(\lambda)$ is the molar absorption coefficient of the acceptor at wavelength λ with unit of $cm^{-1}\,mol^{-1}$. In this study, J was found integrating the overlap of the UV absorption spectrum of DiAmsar and the fluorescence emission spectrum of HSA (or BSA) (Fig. 7), and it was 1.415×10^{-16} and $1.373 \times 10^{-16}\,cm^3\,M^{-1}$ for HSA and BSA, respectively. Energy transfer efficiency E was calculated as 0.49 and 0.40 for HSA and BSA, respectively; Critical energy transfer distance between the donor and acceptor was found to be 1.241 nm for HSA and 1.240 nm for BSA, the distance was found to be 1.250 nm for HSA and 1.235 nm for BSA.

CV spectroscopy studies

The electrochemical behaviour of the DiAmsar was investigated by employing CV in Tris–HCl buffer with pH = 7.4. This research reveals that there are well defined anodic and cathodic peaks at −0.62 and −0.95 mV (Fig. 8(a)). Besides, the CVs of DiAmsar in the presence and absence of HSA and BSA was investigated in Tris–HCl buffer solutions at various concentrations (1.8×10^{-5} M to 4.2×10^{-5} M) and the results are shown in Fig. 8. As can be seen in this figure, significant decrease in peak current and slightly negative shift in anodic peak potential of DiAmsar was observed upon the addition of HSA and BSA, although there were no changes in the cathodic peak potential. Further, no new peaks were noticed in presence of HSA and BSA. These shifts in peak potential indicate that an electro-inactive compound is produced during complex formation.

FT-IR spectroscopy studies

In order to obtain more information on the binding of DiAmsar to HSA and BSA, the FT-IR spectroscopy was investigated. FT-IR spectrum of a protein exhibit a number of amide bands, which represent different vibrations of the peptide moiety. The amide group of proteins and polypeptides presented characteristic vibrational modes (amide modes) that were sensitive to the protein conformation and largely constrained to group frequency interpretations (32). Protein amides I and II bonds appear at 1600–1700 cm^{-1} (mainly C=O stretching) and 1600–1480 cm^{-1} (C-N stretching coupled with N–H bending), which are correlated with structural changes in proteins. Amide I band is more sensitive to the changes in protein secondary structure compared to amide II. Hence, the amide I band is more useful for the study of protein secondary structure (33).

In general, the spectra range in 1650–1660 cm^{-1} in amide I bands can be attributed to α-helix, the range in 1640–1610 cm^{-1}, 1650–1640 cm^{-1} and 1700–1660 cm^{-1} can be ascribed to β-sheet, random coils, and β-turn, respectively. Figure 9 shows the FT-IR spectra of HSA and BSA, which are obtained by subtracting the absorption of the buffer solution from the spectrum of the protein solution and the FT-IR spectra of DiAmsar–HSA (or BSA). It can be found that the secondary structure of HSA and BSA were changed because the peak position of amide I moved from 1637.06 to 1644.36 cm^{-1} for HSA and 1637.27 to 1645.23 cm^{-1} for BSA. After

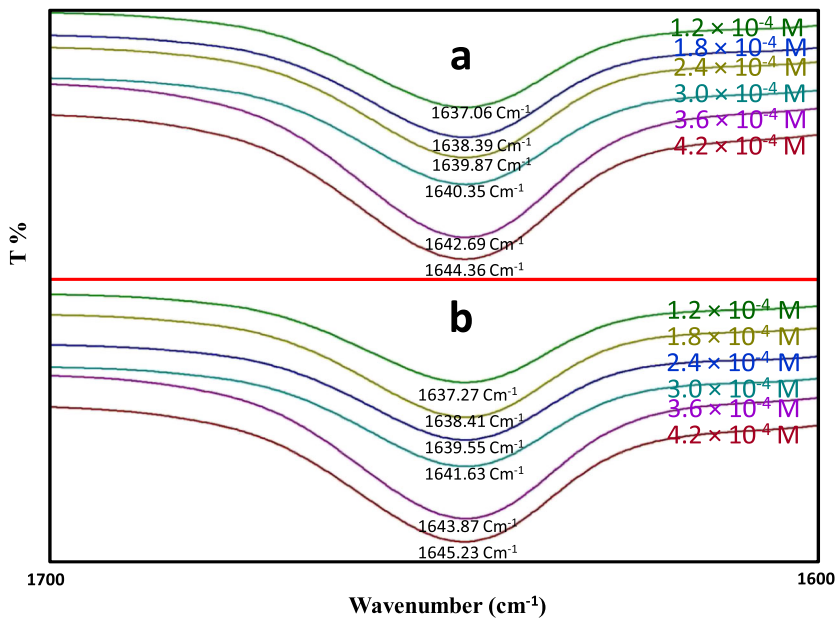

Figure 9. FT-IR spectra of (a) HSA and (b) BSA with different concentrations of DiAmsar.

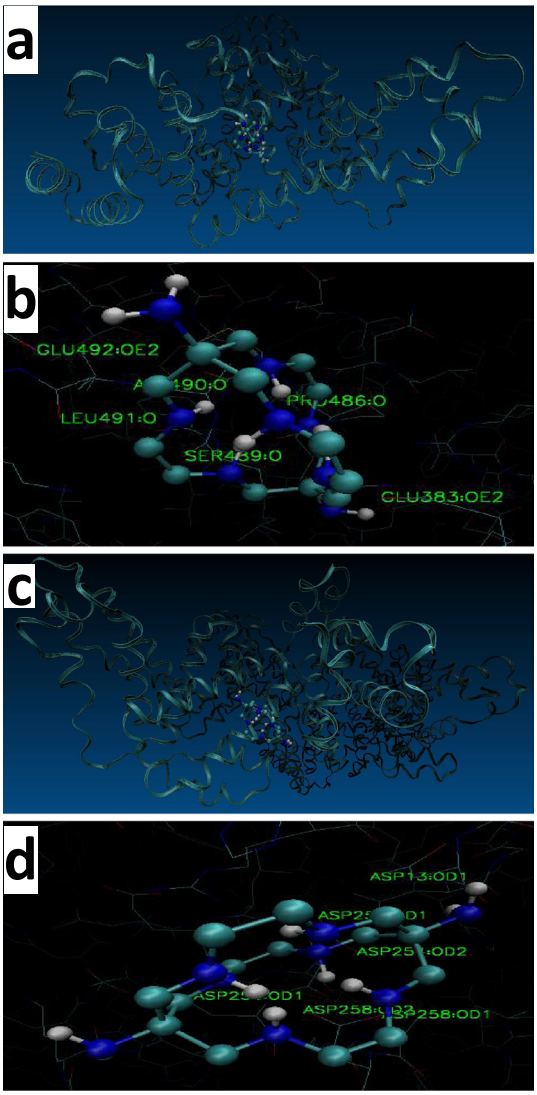

Figure 10. Molecular docking of HSA and BSA with DiAmsar. (a) Ribbons and (b) lines drawing method of HSA with CPK drawing method of DiAmsar; (c) Ribbons and (d) lines drawing method of BSA and CPK drawing method of DiAmsar.

addition of DiAmsar to HSA, the content of β-sheet structures of HSA and BSA changed to random coils structures.

Molecular docking studies

Molecular docking technique is an attractive scaffold to understand the ligand–protein interactions which can substantiate our experimental results. In order to further understand the right site and interaction forces of DiAmsar binding to HSA and BSA, the molecular docking of DiAmsar with HSA and BSA were carried out using AutoDock 4.0 program. The dominating configurations of the binding complex of DiAmsar with HSA and BSA are presented in Fig. 10. As shown in Fig. 10(a, b), there is hydrogen bonding interactions between nitrogen atoms of DiAmsar with PRO486, GLU492, LEU491, SER489, and ALA490 of HSA protein. The free energy change (ΔG°) for binding of the DiAmsar with HSA and BSA found to be –2.98 kcal mol^{-1}. From Fig. 10(d), it can be seen that the DiAmsar molecule is able to form hydrogen bonding with ASP236, ASP255, ASP258, ASP254, and ASP13 of BSA with the –16.87 kcal mol^{-1} binding free energy (ΔG°).

Conclusions

We investigated the nature and magnitude of the interaction of the DiAmsar with HSA and BSA by various spectroscopic (FT-IR, UV–vis, and fluorescence), CV, and molecular docking techniques under physiological conditions. The fluorescence results show that the Stern–Volmer quenching constant K_{SV} is inversely correlated with temperature, which indicates that the probable quenching mechanism of the interaction of DiAmsar with HSA and BSA are initiated by complex formation. It is estimated that HSA and BSA have one binding site that is accessible for DiAmsar, where the DiAmsar–HSA and DiAmsar–BSA complexes are stabilized mainly by hydrophobic forces as indicated by the thermodynamic parameters ($\Delta H^\circ > 0$, and $\Delta S^\circ > 0$) at different temperatures. The binding distances (r) were also obtained according to the FRET. Moreover, the FT-IR spectra results showed that the interaction of DiAmsar with HSA and BSA slightly change the secondary structure of HSA and BSA. Additionally, the results of molecular docking showed that there are hydrogen bonds between DiAmsar and PRO486, GLU492, LEU491, SER489, and ALA490 of HSA protein and ASP236, ASP255, ASP258, ASP254, and ASP13 of BSA.

Acknowledgements

We are grateful to the PNU and INSF for funding this work.

References

1. Liu S, Li D, Huang C, Yap L, Park R, Shan H, et al. The efficient synthesis and biological evaluation of novel bi-functionalized sarcophagine for ^{64}Cu radiopharmaceuticals. Theranostics 2012;2:589–96.
2. Cai H, Fissekis J, Conti PS. Synthesis of a novel bifunctional chelator AmBaSar based on sarcophagine for peptide conjugation and ^{64}Cu radiolabelling, Dalton Trans 2009;27:5395–400.
3. Lears KA, Ferdani R, Liang K, Zheleznyak A, Andrews R, Sherman CD, et al. *In vitro* and *in vivo* evaluation of 64cu-labeled sarar-bombesin analogs in gastrin-releasing peptide receptor–expressing prostate cancer. J Nucl Med 2011;52:470–7.
4. Sargeson AM. Encapsulated metal ions. Pure Appl Chem 1984; 56:1603–19.
5. Bernhardt PV, Harrowfield JM, Kim Y, Lee YH, Park YC. A functionalised macrobicycle complex available for surface immobilisation and protein grafting. Bull Korean Chem Soc 2007;28:589–95.
6. Bottomley GA, Clark IJ, Creaser II, Engelhardt LM, Geue RJ, Hagen KS, et al. The synthesis and structure of encapsulating ligands: properties of bicyclic hexamines. Aust J Chem 1994;47:143–79.
7. Voss SD, Smith SV, DiBartolo N, McIntosh LJ, Cyr EM, Bonab AA, et al. Positron emission tomography (PET) imaging of neuroblastoma and melanoma with ^{64}Cu-SarAr immunoconjugates. Proc Natl Acad Sci U S A 2007;104:17489–93.
8. Wadas TJ, Wong EH, Weisman GR, Anderson CJ. Copper chelation chemistry and its role in copper radiopharmaceuticals. Curr Pharm Des 2007;13:3–16.
9. Wei L, Ye Y, Wadas TJ, Lewis JS, Welch MJ, Achilefu S, et al. ^{64}Cu-labeled cb-te2a and DiAmsar conjugated rgd peptide analogs for targeting angiogenesis: comparison of their biological activity. Nucl Med Biol 2009;36:277–85.
10. Cai H, Li Z, Huang CW, Park R, Shahinian AH, Conti PS. An improved synthesis and biological evaluation of a new cage-like bifunctional chelator, 4-((8-amino-3,6,10,13,16,19-hexaazabicyclo6.6.6]icosane-1-ylamino)methyl)benzoic acid, for ^{64}Cu radiopharmaceuticals. Nucl Med Biol 2010;37:57–65.
11. Christian GJ, Arbuse A, Fontrodona X, Martinez MA, Llobet A, Maseras F. Oxidative dehydrogenation of an amine group of a macrocyclic ligand in the coordination sphere of a CuII complex. Dalton Trans 2009;6013–20.
12. Grøndahl L, Hammershøi A, Sargeson AM, Thom VJ. Stability and kinetics of acid- and anion-assisted dissociation reactions of

LUMINESCENCE
The Journal of Biological and Chemical Luminescence

hexaamine macrobicyclic mercury(II) complexes. Inorg Chem 1997;36:5396–403.
13. Bardajee GR, Hooshyar Z, Khanjari M. Dye fluorescence quenching by newly synthesized silver nanoparticles. J Photochem Photobiol A 2013;276:113–21.
14. Hall MD, Failes TW, Yamamoto N, Hambley TW. Bioreductive activation and drug chaperoning in cobalt pharmaceuticals. Dalton Trans 2007;3983–90.
15. Pérez M, Wappner P, Quesada-Allué LA. Catecholamine-β-alanyl ligase in the medfly Ceratitis capitata Insect. Biochem Molec Biol 2002;32:617–25.
16. Mroziński J, Skorupa A, Pochaba A, Dromzée Y, Verdaguer M, Goovaerts E, et al. Sarcophagine Ni(II) diperchlorate: synthesis, crystallographic structure, magnetism and high-field EPR. J Mol Struct 2001;559:107–18.
17. Savadkoohi S, Bannikova A, Kasapis S, Adhikari B. Structural behaviour in condensed bovine serum albumin systems following application of high pressure. Food Chem 2014;150:469–76.
18. Lin J, Liu Y, Chen M, Huang H, Song L. Investigation on the binding activities of citalopram with human and bovine serum albumins. J Lumin 2014;146:114–22.
19. Osaki F, Goto T, Lee SH, Oe T. Predicted multiple selected reaction monitoring to screen activated drug-mediated modifications on human serum albumin. Anal Biochem 2014;449:59–67.
20. Ueno HM, Urazono H, Kobayashi T. Serum albumin forms a lactoferrin-like soluble iron-binding complex in presence of hydrogen carbonate ions. Food Chem 2014;145:90–4.
21. Zhang X, Zhai H, Gao R, Zhang J, Zhang Y, Zheng X. Study on the interaction between 4-thio-5-methyluridine and human serum albumin by spectroscopy and molecular modeling. Spectrochim Acta A Mol Biomol Spectrosc 2014;121:724–31.
22. Fu L, Liu X, Zhou Q, Zhang J, Dong J, Wang J. Characterization of the interactions of human serum albumin (HSA), gatifloxacin, and metronidazole using spectroscopic and electrochemical methods. J Lumin 2014;149:208–14.
23. Asadi M, Asadi Z, Sadi SB, Zarei L, Baigi FM, Amirghofran Z. Synthesis, characterization and the interaction of some new water-soluble metal Schiff base complexes with human serum albumin. Spectrochim Acta A Mol Biomol Spectrosc 2014;122:118–29.
24. Guo X, Li X, Jiang Y, Yi L, Wu Q, Chang H, et al. A spectroscopic study on the interaction between p-nitrophenol and bovine serum albumin. J Lumin 2014;149:353–60.
25. Shahabadi N, Khorshidi A, Moghadam NH. Study on the interaction of the epilepsy drug, zonisamide with human serum albumin (HSA) by spectroscopic and molecular docking techniques. Spectrochim Acta A Mol Biomol Spectrosc 2013;114:627–32.
26. Fani N, Bordbar AK, Ghayeb Y. Spectroscopic, docking and molecular dynamics simulation studies on the interaction of two Schiff base complexes with human serum albumin. J Lumin 2013;141:166–72.
27. Zhao X, Liu R, Teng Y, Liu X. The interaction between Ag^{+} and bovine serum albumin: A spectroscopic investigation. Sci Total Environ 2011;409:892–7.
28. Zhao X, Sheng F, Zheng J, Liu R. Composition and stability of anthocyanins from Purple Solanum Tuberosum and their protective influence on Cr(VI) targeted to bovine serum albumin. J Agric Food Chem 2011;59:7902–9.
29. Zhao X, Liu R, Chi Z, Teng Y, Qin P. New insights into the behavior of bovine serum albumin adsorbed onto carbon nanotubes: Comprehensive spectroscopic studies. J Phys Chem B 2010;114:5625–31.
30. Bogdan M, Pirnau A, Floare C, Bugeac C. Binding interaction of indomethacin with human serum albumin. J Pharm Biomed Anal 2008;47:981–4.
31. Barbero N, Barni E, Barolo C, Quagliotto P, Viscardi G, Napione L, et al. A study of the interaction between fluorescein sodium salt and bovine serum albumin by steady-state fluorescence. Dyes Pigment 2009;80:307–13.
32. Dong X, Zhou R, Jing H. Characterization and antioxidant activity of bovine serum albumin and sulforaphane complex in different solvent systems. J Lumin 2014;146:351–7.
33. Shahabadi N, Maghsudi M, Kiani Z, Pourfoulad M. Multispectroscopic studies on the interaction of 2-tert-butylhydroquinone (TBHQ), a food additive, with bovine serum albumin. Food Chem 2011;124:1063–8.

